Experimental study of subwavelength grating bimodal waveguides as ultrasensitive interferometric sensors

L. TORRIJOS-MORÁN, A. GRIOL AND J. GARCÍA-RUPÉREZ*

Nanophotonics Technology Center, Universitat Politècnica de València, Camino de Vera s/n, 46022 Valencia, Spain
**Corresponding author: jaigarru@ntc.upv.es*

Received XX Month XXXX; revised XX Month, XXXX; accepted XX Month XXXX; posted XX Month XXXX (Doc. ID XXXXX); published XX Month XXXX

During the last years, subwavelength grating (SWG) structures are gaining increasing attention in the area of evanescent-field photonic sensors. Here, we present for the first time an experimental demonstration of real-time refractive index (RI) sensing using SWG bimodal interferometric structures. Two different configurations are considered in order to compare the effect of the non-linear phase shift, obtained between the two first TE propagating modes, in the measured bulk sensitivity. Very high experimental values up to 2270nm/RIU are reached, which perfectly match the numerical simulations and significantly enhance other existing SWG and spectral-based sensors. By measuring the spectral shift, the experimental sensitivity obtained does not depend on the sensor length. As a result, a highly sensitive and compact single-channel interferometer is experimentally validated for RI sensing, opening new possible paths in the field of optical integrated sensors.

http://dx.doi.org/10.1364/OL.99.099999

A periodic dielectric configuration having a lattice constant being smaller than the wavelength of light can be considered as a homogeneous anisotropic material in which electromagnetic wave propagation is feasible [1]. This is the case of the so-called subwavelength gratings (SWGs), firstly described in [2–4] as an alternative type of silicon waveguides and later on extended to all kind of integrated photonic applications [5,6]. More recently, SWG structures have been reported in the literature for refractive index (RI) sensing [7], providing very high bulk and surface sensitivities due to a stronger light-matter interaction with the surrounding media than for conventional waveguides. As a consequence, several sensor configurations such as ring resonators (RR) have been redesigned using SWG structures [8–11], exhibiting a superior performance in terms of both sensitivity and limit of detection. Moreover, SWG also offer additional dispersive properties [12] that can be exploited to develop, for instance, broadband directional couplers [13], beam-splitters [14], polarization controllers [15] and densely integrated waveguides [16]. Within this context, we proposed in a previous work the use of a bimodal SWG waveguide as a spectral-interrogation based sensor [17], where high sensitivity values were theoretically obtained as a result of the inherent dispersive behavior of SWG structures. On the other hand, similar single-channel interferometers in homogeneous structures have been extensively studied and validated for biosensing purposes [18–20]. In these cases, the sensing performance has been determined by measuring the phase shift, which scales directly with the sensor length, and with the main drawback that large dimensions are required to reach high sensitivities.

In this letter, we experimentally demonstrate for the first time the use of SWG bimodal waveguides as high performance single-channel interferometric sensors. The underlying idea is to take advantage of the SWG dispersion properties to enhance the spectral shift of a certain interference dip in the spectra. As a result, we show an experimental bulk sensitivity of 2270nm/RIU for a compact SWG bimodal device being only ~125μm long.

The sketch of the proposed configuration is depicted in Fig. 1(a), where a single transverse electromagnetic (TE) mode waveguide, acting as input port, excites the first two TE modes of the bimodal SWG waveguide. Similarly, these two modes will contribute to the excitation of the fundamental mode of the output single-mode waveguide. At this point, the transferred power will depend on the phase shift between the propagating modes of the SWG structure, creating an interference pattern in the transmission spectrum. By tracking the position of a certain spectral dip in the spectrum, caused by a destructive interference between both modes, we can determine the sensitivity of the sensor under different bulk RI variations. In this kind of spectral-interrogation based sensors, bulk sensitivity can be mathematically expressed as follows [17]:

$$S_b = \frac{\partial \lambda_f}{\partial n_c} = \frac{\partial \varphi / \partial n_c}{\partial \varphi / \partial \lambda_f}, \quad (1)$$

where $\partial\lambda_f$ is the differential shift of the spectral dip in nm, ∂n_c is the differential RI change of the cladding in refractive index units (RIU) and $\partial\varphi$ is the differential phase shift in radians between the two interfering modes. According to Eq. (1), low slopes of the phase shift as a function of wavelength will increase the sensitivity

of the interferometer [21]. The dispersion diagrams of the periodic SWG structures created on silicon (n=3.47) over a silica substrate (n=1.44) have been computed using MIT Photonics Bands (MPB) free software (see Fig. 1(b)). The design dimensions are: SWG bimodal waveguide width w_{swg}=1400nm, height h=220nm, lattice period Λ_1=260nm and transversal elements width w_i=160nm. In the beginning of the bimodal region, around 1500nm, the even mode is more dispersive than the odd one. In contrast, for higher wavelengths the even mode becomes less dispersive than the odd mode, producing lower slopes of the phase shift as a function of wavelength, as it is shown in Fig. 1(c). This fact will provoke high wavelength shifts for those spectral features located at the low-slope wavelength regions. By using different SWG periodicity values, we can tune where this effect occurs and study its influence in the shift of the spectral dips. In Fig. 1(c) we show the evolution of the phase shift as a function of wavelength for Λ_1=260nm, w_i=160nm and a secondary design of Λ_2=280nm and w_i=180nm. At higher wavelengths, the slope of both configurations decreases, what will be translated into high spectral shifts of the dips, as indicated by Eq. (1). Nonetheless, for standard operating wavelengths around 1550nm this effect will be theoretically higher for the SWG structure of Λ_1=260nm, since we are working in a flatter phase shift region than for the Λ_2=280nm configuration.

For the experimental demonstration, the sensor has been accessed in and out with a single-mode waveguide of width w_s=450nm. Due to symmetry conditions of the modes field distribution (see Fig. 1(d)), the access single-mode waveguides must be displaced a certain distance "d" with respect to the x=0 point, in order to excite the odd parity mode in the SWG region (see Fig. 1(e)). A displaced distance d=350nm has been used for an optimal excitation of both SWG modes.

These designed SWG structures have been fabricated on a silicon-on-insulator (SOI) wafer with an upper silicon layer thickness of 220nm and a buried silica layer of 2µm. Electron beam lithography, with an acceleration voltage of 30KeV and an aperture size of 30µm, has been used in the exposure process on a HSQ negative resist, and inductively coupled plasma etching of the top silicon layer has been employed to transfer the resist patterns into the SOI wafer. Scanning electron microscope (SEM) images of the fabricated SWG sensors are depicted in Fig. 1(d) and (e).

The optical characterization of the fabricated sensors has been carried out using a coherent TE polarized light from a tunable laser (Keyshight 81980) that has been vertically coupled into the chip by using grating couplers. Light collected at the output is measured using an optical power meter (Keyshight 81636B) that is synchronized with the laser sweep. A LabVIEW application has been programmed to continuously save the spectrum data, and thus being able to perform time evolution experiments.

First results of the transmission spectra are shown in Fig. 2(a) for a SWG structure of N=480 elements, normalized respect to a uniform reference waveguide in dB units. The sensor has been covered with pure deionized water (DIW) and with a dilution of 6% ethanol (EtOH) volume in DIW, added gradually on the initial pure DIW dilution to obtain the desired concentrations. The dilutions have been directly dropped onto the sample and measured afterwards. According to [22], the RI of these dilutions can be linearly approximated (in mass) for these working conditions (λ=1550nm at 25ºC), obtaining a value of n_{DIW}=1.3173 and $n_{EtOH(6\%)}$=1.3205. The experimental data present a ripple, as a consequence of the Fabry-Perot resonances produced in the SWG

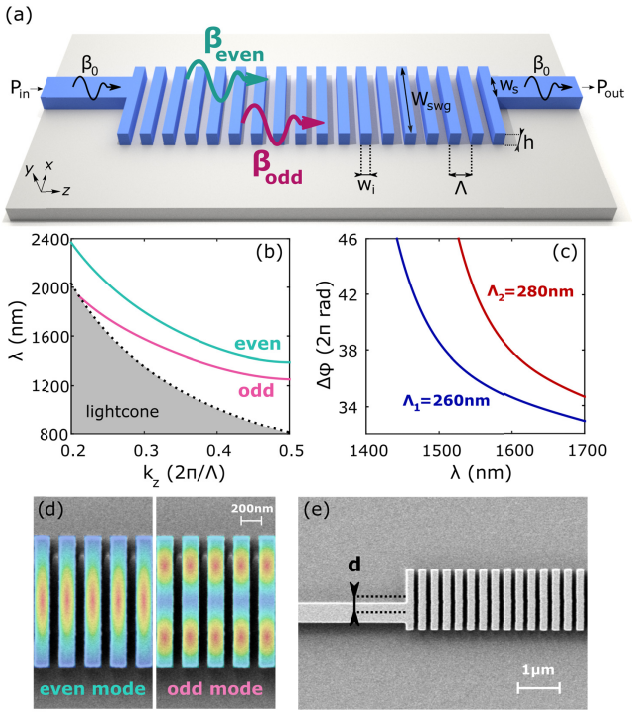

Fig. 1. (a) Sketch of the proposed bimodal SWG sensor and its design parameters. (b) Dispersion diagram of even and odd modes with w=1400nm, h=220nm, Λ_1=260nm and w_i=160nm. (c) Phase shift '$\Delta\varphi = L*(\beta_{even}-\beta_{odd})$' between the even and odd modes as a function of wavelength for Λ_1 and Λ_2 configurations, and N=480 elements. (d) Electric field energy density of the TE even and odd modes excited in the SWG bimodal region. They are depicted over a SEM image of the fabricated structure. (e) SEM image of the interface between the SWG bimodal waveguide and the single-mode access waveguide, showing an input-output displacement distance of d=350nm.

discontinuities, that could have a negative effect on the limit of detection since the minimum of the spectral response could not be easily tracked in future biosensing experiments. For that reason, a Lorentzian fitting has been applied to the raw data of each spectral dip in order to better follow the evolution of the minimum. As it was theoretically predicted in [17], the spectral dips are shifted towards lower wavelengths when the RI of the dilution increases (see Fig. 2(a)). Additionally, it can be seen how the absolute wavelength shift of the spectra for Λ_1=260nm is higher than that obtained for the spectra of Λ_2=280nm. This is due to the lower phase shift slope as a function of wavelength obtained for the Λ_1 configuration in comparison with the Λ_2 configuration and for our experimental wavelength range, as previously described. Besides, note that the spectral shift in both configurations is lower as we decrease in wavelength, what indicates the high dependence of the sensitivity with the dip spectral position.

Conversely, a greater number of spectral dips is experimentally observed in Fig. 2(a) for the configuration with Λ_2=280nm compared to the other with Λ_1=260nm, in the same range of wavelengths. This is explained by the higher phase shift slope obtained for the Λ_2 configuration that produces more destructive interferences than the Λ_1 configuration in the same bandwidth. As a consequence, the spectral dips will be narrower for the Λ_2 configuration and thus easier to track in future sensing experiments. More specifically, for the Λ_2=280nm configuration

the full width at half maximum (FWHM) of the most sensitive spectral dip located at 1580nm is twice that for the lowest dip at 1523nm. Therefore, a trade-off between sensitivity and narrower spectral dips is observed, although the FWHM of the most sensitive dips could be reduced by increasing the number of elements N.

In order the compare results with simulations, the dispersion relations of both SWG modes have been computed under different cladding RI scenarios of pure DIW and 6% ethanol volume in DIW. The computed absolute wavelength shift of each spectral dip and the experimental results are depicted in Fig. 2(b) for both configurations, showing a good agreement between theory and measurements for a RI increment of 3.2×10^{-3}RIU. Moreover, it should be noted again that in Fig. 2(b) the shift is strongly dependent on wavelength because of the non-linear phase shift behavior of the SWG structure. This fact provokes higher sensitivities for those spectral dips located at higher wavelengths.

Likewise, several time evolution measurements have been carried out by covering the SWG sensor with different ethanol dilutions. To this end, real-time spectrum data has been collected for 35 minutes and subsequently processed to properly track the minimum of each spectral dip over time. Figure 3(a) shows the tracking of the spectral dip located at 1580nm for Λ_1=260nm and Λ_2=280nm configurations. Ethanol dilutions of 2%, 4% and 6% in DIW have been considered for the experiments, corresponding to a RI of 1.3183, 1.3194 and 1.3205, respectively. The absolute wavelength shift versus RI variations is depicted in Fig. 3(b) for both configurations. In this graph, we obtain a bulk sensitivity of 2270nm/RIU for the SWG configuration with Λ_1=260nm and a value of 1253nm/RIU for the SWG with Λ_2=280nm. These results are in good agreement with the numerically simulations previously calculated and are consistent with the phase shift slopes presented in Fig. 1(c). Note that there is a period of time that the measurements take to stabilize, this is due to the RI variations occurring when new ethanol dilutions are added.

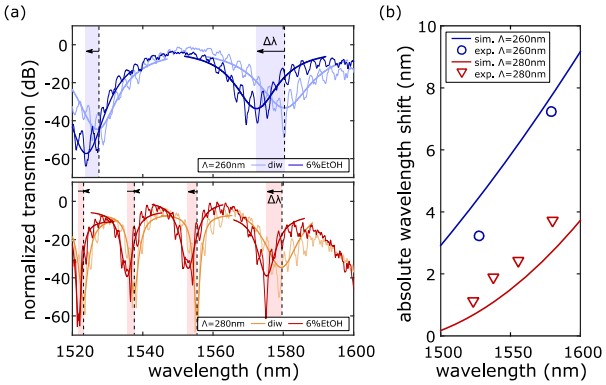

Fig. 2. (a) Experimental normalized transmission spectra respect to a reference waveguide, obtained for a bimodal SWG sensor of N=480 elements, Λ_1=260nm, w_i=160nm (upper blue graph) and Λ_2=280nm, w_i=180nm (lower red graph). A Lorentzian fitting is also depicted over the spectral dips to ease the determination of the minimum location. (b) Experimental comparison between the numerical simulations and the absolute wavelength shifts of each spectral dip for a refractive index change of 3.2×10^{-3}RIU as a function of wavelength, and for periods of Λ_1=260nm and Λ_2=280nm. The lines show the numerical simulations for a continuous range of wavelengths and the markers show the experimental values of each spectral dip located at a certain wavelength.

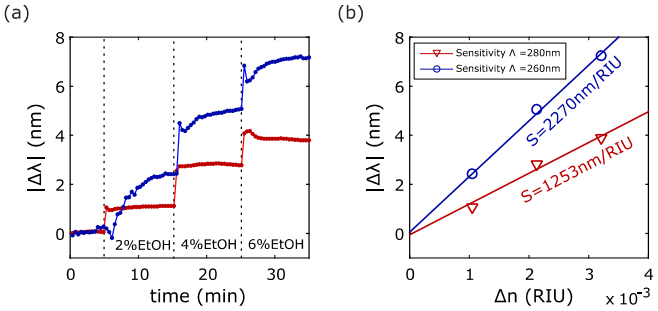

Fig. 3. (a) Time evolution of the spectral dips located at 1580nm with N=480 elements for Λ_1=260nm, w_i=160nm (blue curve) and Λ_2=280nm, w_i=180nm (red curve) under three different dilutions of 2%, 4% and 6% of ethanol volume in DIW. (b) Representation of the absolute wavelength shift of the spectral dips under different RI variations. The linear fitting represents the bulk sensitivity experimentally obtained for both configurations.

In comparison with the literature, SWG spectral based sensors such as multi-box ring resonators [23] have reported an experimental bulk sensitivity of 580nm/RIU, and other configurations like slot ring resonators [24] have been experimentally demonstrated for RI sensing with sensitivities up to 1300nm/RIU; as well as slotted photonic crystal sensors [25] with a reported sensitivity of 1538nm/RIU. On the other hand, similar bimodal interferometers [26] using homogeneous waveguides have been presented as spectral based sensors with sensitivity values of 789nm/RIU. Therefore, our proposed sensor presents a markedly higher bulk sensitivity than previous examples while keeping a very low structural complexity, thus confirming the high potential of SWG bimodal waveguides as a promising alternative for sensing applications in CMOS-compatible integrated devices.

To investigate the dependence of the experimental sensitivity with the sensor length, the spectral shift of several dips with SWG configurations of N=120, N=240, N=360 and N=480 elements for a RI change of 5.39×10^{-3}RIU has been also measured. The rest of the design parameters are the same used in the previous analysis (w_s=450nm, w=1400nm, h=220nm, d=350nm, Λ_2=280nm and w_i=180nm). Figure 4(a) depicts numerical simulations for the numerator and the denominator of Eq. (1), varying the number N of SWG elements. In this graph we can clearly see that the value of the numerator and denominator highly depends on N and wavelength. However, when we apply Eq. (1) and divide both expressions, the theoretical sensitivity obtained remains constant for any value of N, although it still depends on wavelength. This theoretical sensitivity curve is shown in Fig. 4(b) as a function of wavelength. The colored bars represent the experimental sensitivity of each spectral dip obtained for different N at a certain wavelength. All the measurements are in a good agreement with the simulations and remain on the line of Eq. (1). These results demonstrate that the bulk sensitivity, measuring the wavelength shift, does not depend on the sensor length, as it occurs in interferometric configurations when measuring the phase shift.

Despite this, as it has been explained before, the quality factor of the spectral dip increases with N since they are more grouped in the spectrum and narrower spectral features are obtained. As a result, longer SWG structures will facilitate the tracking of those dips and thus enhance the limit of detection of the sensor, although it will increase its footprint, which is not very suitable for

integration purposes. Future optimized designs must be made in order to enhance the sensor limit of detection, and thus compare it to other existing devices in biosensing applications [27]. The obtained transmission spectra for different N have been compared to the one recorded with a single-mode waveguide, with the aim of measuring the insertion losses of the sensor. A value around 1dB has been obtained for any number of elements N, which means that losses are mainly due to the coupling between the single-mode access waveguides and the bimodal SWG and that propagation losses can be considered practically negligible, thus allowing the use of long bimodal SWG sections if desired.

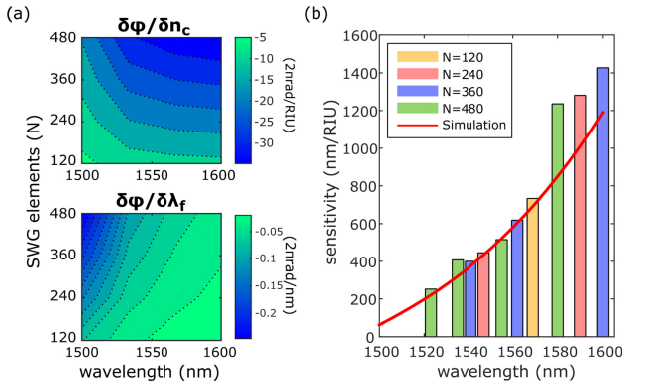

Fig. 4. (a) Color map representing the numerical derivative of the phase shift with respect to the cladding RI (upper graph) and wavelength (lower graph), for different number of periods N and wavelengths. (b) Comparison between the simulated sensitivity obtained using Eq. (1) (red curve) and the experimental results considering different number of periods N (colored bars). The SWG dimensions used for the simulation and experimental measurements are w=1400nm, h=220nm, d=350nm, Λ_2=280nm and w_i=180nm.

To conclude, we have demonstrated the use of bimodal SWG waveguides for RI sensing and studied their high-performance experimental features. The proposed mechanism relies on the dispersive behavior of SWG structures to critically enhance the wavelength shift of the spectral dips when varying the RI of the cladding. A complete comparison of experimental results and simulations is provided, as well as time evolution measurements to evaluate its bulk sensitivity. Values up to 2270nm/RIU have been obtained for a SWG periodicity and element width of 260nm and 160nm, respectively. To the best of our knowledge, these experimental results are the highest reported in the literature for an integrated silicon RI sensor. Furthermore, its scalable properties allow us to design the sensor to work at the desired wavelength by simply changing the lattice period of the structure. Overall, its compact full-etched single-channel design and its outstanding sensitivity, places it as a promising alternative for lab-on-a-chip devices in future work.

Funding. This work was funded by the European Commission through the Horizon 2020 Programme (PHC-634013 PHOCNOSIS project), the Spanish government through the project TEC2015-63838-C3-1-R-OPTONANOSENS and Universitat Politècnica de València through grant PAID 01-18.

References

1. S. M. Rytov, JETP, Sov. Phys. **2**, 466 (1956).
2. P. Cheben, D.-X. Xu, S. Janz, and A. Densmore, Opt. Express **14**, 4695 (2006).
3. D.-X. Xu, E. Post, J. Lapointe, P. Cheben, S. Janz, and J. H. Schmid, Opt. Lett. **32**, 1794 (2007).
4. P. J. Bock, P. Cheben, J. H. Schmid, J. Lapointe, A. Delâge, S. Janz, G. C. Aers, D.-X. Xu, A. Densmore, and T. J. Hall, Opt. Express **18**, 20251 (2010).
5. R. Halir, P. J. Bock, P. Cheben, A. Ortega-Moñux, C. Alonso-Ramos, J. H. Schmid, J. Lapointe, D. X. Xu, J. G. Wangüemert-Pérez, Í. Molina-Fernández, and S. Janz, Laser Photonics Rev. **9**, 25 (2015).
6. P. Cheben, R. Halir, J. H. Schmid, H. A. Atwater, and D. R. Smith, Nature **560**, 565 (2018).
7. J. Gonzalo Wangüemert-Pérez, P. Cheben, A. Ortega-Moñux, C. Alonso-Ramos, D. Pérez-Galacho, R. Halir, I. Molina-Fernández, D.-X. Xu, and J. H. Schmid, Opt. Lett. **39**, 4442 (2014).
8. V. Donzella, A. Sherwali, J. Flueckiger, S. M. Grist, S. T. Fard, and L. Chrostowski, Opt. Express **23**, 4791 (2015).
9. J. Flueckiger, S. Schmidt, V. Donzella, A. Sherwali, D. M. Ratner, L. Chrostowski, and K. C. Cheung, Opt. Express **24**, 15672 (2016).
10. H. Yan, L. Huang, X. Xu, S. Chakravarty, N. Tang, H. Tian, and R. T. Chen, Opt. Express **24**, 29724 (2016).
11. H. Tian, H. Yan, N. Tang, R. T. Chen, S. Chakravarty, L. Huang, and X. Xu, Opt. Express **25**, 10527 (2017).
12. D. Benedikovic, M. Berciano, C. Alonso-Ramos, X. Le Roux, E. Cassan, D. Marris-Morini, and L. Vivien, Opt. Express **25**, 19468 (2017).
13. Y. Wang, Z. Lu, M. Ma, H. Yun, F. Zhang, N. A. F. Jaeger, and L. Chrostowski, IEEE Photonics J. **8**, 1 (2016).
14. R. Halir, P. Cheben, J. M. Luque-González, J. D. Sarmiento-Merenguel, J. H. Schmid, G. Wangüemert-Pérez, D. X. Xu, S. Wang, A. Ortega-Moñux, and Í. Molina-Fernández, Laser Photonics Rev. **10**, 1039 (2016).
15. J. M. Luque-González, A. Herrero-Bermello, A. Ortega-Moñux, Í. Molina-Fernández, A. V. Velasco, P. Cheben, J. H. Schmid, S. Wang, and R. Halir, Opt. Lett. **43**, 4691 (2018).
16. S. Jahani, S. Kim, J. Atkinson, J. C. Wirth, F. Kalhor, A. Al Noman, W. D. Newman, P. Shekhar, K. Han, V. Van, R. G. Decorby, L. Chrostowski, M. Qi, and Z. Jacob, Nat. Commun. **9**, (2018).
17. L. Torrijos-Morán and J. García-Rupérez, Opt. Express **27**, 8168 (2019).
18. R. Levy and S. Ruschin, IEEE Sens. J. **9**, 146 (2009).
19. K. E. Zinoviev, A. B. González-Guerrero, C. Domínguez, and L. M. Lechuga, J. Light. Technol. **29**, 1926 (2011).
20. P. Kozma, F. Kehl, E. Ehrentreich-Förster, C. Stamm, and F. F. Bier, Biosens. Bioelectron. **58**, 287 (2014).
21. R. Levy and S. Ruschin, Opt. Express **16**, 20516 (2008).
22. J. García-Rupérez, V. Toccafondo, M. J. Bañuls, J. G. Castelló, A. Griol, S. Peransi-Llopis, and Á. Maquieira, Opt. Express **18**, 24276 (2010).
23. E. Luan, H. Yun, L. Laplatine, K. Cheung, Y. Dattner, D. Ratner, J. Flückiger, and L. Chrostowski, Integr. Opt. Devices, Mater. Technol. XXII **10535**, 105350H (2018).
24. W. Zhang, S. Serna, X. Le Roux, L. Vivien, and E. Cassan, Opt. Lett. **41**, 532 (2016).
25. A. Di Falco, L. O'Faolain, and T. F. Krauss, Appl. Phys. Lett. **94**, 92–95 (2009).
26. Y. Liang, M. Zhao, Z. Wu, and G. Morthier, IEEE Photonics J. **11**, (2019).
27. Í. Molina-Fernández, J. Leuermann, A. Ortega-Moñux, J. G. Wangüemert-Pérez, and R. Halir, Opt. Express **27**, 12616 (2019).

Full reference list:

1. S. M. Rytov, "Electromagnetic properties of a finely stratified medium," JETP, Sov. Phys. **2**, 466–475 (1956).
2. P. Cheben, D.-X. Xu, S. Janz, and A. Densmore, "Subwavelength waveguide grating for mode conversion and light coupling in integrated optics," Opt. Express **14**, 4695 (2006).
3. D.-X. Xu, E. Post, J. Lapointe, P. Cheben, S. Janz, and J. H. Schmid, "Gradient-index antireflective subwavelength structures for planar waveguide facets," Opt. Lett. **32**, 1794 (2007).
4. P. J. Bock, P. Cheben, J. H. Schmid, J. Lapointe, A. Delâge, S. Janz, G. C. Aers, D.-X. Xu, A. Densmore, and T. J. Hall, "Subwavelength grating periodic structures in silicon-on-insulator: a new type of microphotonic waveguide," Opt. Express **18**, 20251–20262 (2010).
5. R. Halir, P. J. Bock, P. Cheben, A. Ortega-Moñux, C. Alonso-Ramos, J. H. Schmid, J. Lapointe, D. X. Xu, J. G. Wangüemert-Pérez, Í. Molina-Fernández, and S. Janz, "Waveguide sub-wavelength structures: A review of principles and applications," Laser Photonics Rev. **9**, 25–49 (2015).
6. P. Cheben, R. Halir, J. H. Schmid, H. A. Atwater, and D. R. Smith, "Subwavelength integrated photonics," Nature **560**, 565–572 (2018).
7. J. Gonzalo Wangüemert-Pérez, P. Cheben, A. Ortega-Moñux, C. Alonso-Ramos, D. Pérez-Galacho, R. Halir, I. Molina-Fernández, D.-X. Xu, and J. H. Schmid, "Evanescent field waveguide sensing with subwavelength grating structures in silicon-on-insulator," Opt. Lett. **39**, 4442–4445 (2014).
8. V. Donzella, A. Sherwali, J. Flueckiger, S. M. Grist, S. T. Fard, and L. Chrostowski, "Design and fabrication of SOI micro-ring resonators based on sub-wavelength grating waveguides," Opt. Express **23**, 4791 (2015).
9. J. Flueckiger, S. Schmidt, V. Donzella, A. Sherwali, D. M. Ratner, L. Chrostowski, and K. C. Cheung, "Sub-wavelength grating for enhanced ring resonator biosensor," Opt. Express **24**, 15672–15686 (2016).
10. H. Yan, L. Huang, X. Xu, S. Chakravarty, N. Tang, H. Tian, and R. T. Chen, "Unique surface sensing property and enhanced sensitivity in microring resonator biosensors based on subwavelength grating waveguides," Opt. Express **24**, 29724 (2016).
11. H. Tian, H. Yan, N. Tang, R. T. Chen, S. Chakravarty, L. Huang, and X. Xu, "Improving the detection limit for on-chip photonic sensors based on subwavelength grating racetrack resonators," Opt. Express **25**, 10527 (2017).
12. D. Benedikovic, M. Berciano, C. Alonso-Ramos, X. Le Roux, E. Cassan, D. Marris-Morini, and L. Vivien, "Dispersion control of silicon nanophotonic waveguides using sub-wavelength grating metamaterials in near- and mid-IR wavelengths," Opt. Express **25**, 19468–19478 (2017).
13. Y. Wang, Z. Lu, M. Ma, H. Yun, F. Zhang, N. A. F. Jaeger, and L. Chrostowski, "Compact Broadband Directional Couplers Using Subwavelength Gratings," IEEE Photonics J. **8**, 1–8 (2016).
14. R. Halir, P. Cheben, J. M. Luque-González, J. D. Sarmiento-Merenguel, J. H. Schmid, G. Wangüemert-Pérez, D. X. Xu, S. Wang, A. Ortega-Moñux, and Í. Molina-Fernández, "Ultra-broadband nanophotonic beamsplitter using an anisotropic sub-wavelength metamaterial," Laser Photonics Rev. **10**, 1039–1046 (2016).
15. J. M. Luque-González, A. Herrero-Bermello, A. Ortega-Moñux, Í. Molina-Fernández, A. V. Velasco, P. Cheben, J. H. Schmid, S. Wang, and R. Halir, "Tilted subwavelength gratings: controlling anisotropy in metamaterial nanophotonic waveguides," Opt. Lett. **43**, 4691–4694 (2018).
16. S. Jahani, S. Kim, J. Atkinson, J. C. Wirth, F. Kalhor, A. Al Noman, W. D. Newman, P. Shekhar, K. Han, V. Van, R. G. Decorby, L. Chrostowski, M. Qi, and Z. Jacob, "Controlling evanescent waves using silicon photonic all-dielectric metamaterials for dense integration," Nat. Commun. **9**, (2018).
17. L. Torrijos-Morán and J. García-Rupérez, "Single-channel bimodal interferometric sensor using subwavelength structures," Opt. Express **27**, 8168–8179 (2019).
18. R. Levy and S. Ruschin, "Design of a single-channel modal interferometer waveguide sensor," IEEE Sens. J. **9**, 146–153 (2009).
19. K. E. Zinoviev, A. B. González-Guerrero, C. Domínguez, and L. M. Lechuga, "Integrated bimodal waveguide interferometric biosensor for label-free analysis," J. Light. Technol. **29**, 1926–1930 (2011).
20. P. Kozma, F. Kehl, E. Ehrentreich-Förster, C. Stamm, and F. F. Bier, "Integrated planar optical waveguide interferometer biosensors: A comparative review," Biosens. Bioelectron. **58**, 287–307 (2014).
21. R. Levy and S. Ruschin, "Critical sensitivity in hetero-modal interferometric sensor using spectral interrogation.," Opt. Express **16**, 20516–20521 (2008).
22. J. García-Rupérez, V. Toccafondo, M. J. Bañuls, J. G. Castelló, A. Griol, S. Peransi-Llopis, and Á. Maquieira, "Label-free antibody detection using band edge fringes in SOI planar photonic crystal waveguides in the slow-light regime.," Opt. Express **18**, 24276–24286 (2010).
23. E. Luan, H. Yun, L. Laplatine, K. Cheung, Y. Dattner, D. Ratner, J. Flückiger, and L. Chrostowski, "Sub-wavelength multi-box waveguide-based label-free sensors," Integr. Opt. Devices, Mater. Technol. XXII **10535**, 105350H (2018).
24. W. Zhang, S. Serna, X. Le Roux, L. Vivien, and E. Cassan, "Highly sensitive refractive index sensing by fast detuning the critical coupling condition of slot waveguide ring resonators," Opt. Lett. **41**, 532–535 (2016).
25. A. Di Falco, L. O'Faolain, and T. F. Krauss, "Chemical sensing in slotted photonic crystal heterostructure cavities," Appl. Phys. Lett. **94**, 92–95 (2009).
26. Y. Liang, M. Zhao, Z. Wu, and G. Morthier, "Bimodal Waveguide Interferometer RI Sensor Fabricated on Low-Cost Polymer Platform," IEEE Photonics J. **11**, (2019).
27. Í. Molina-Fernández, J. Leuermann, A. Ortega-Moñux, J. G. Wangüemert-Pérez, and R. Halir, "Fundamental limit of detection of photonic biosensors with coherent phase read-out," Opt. Express **27**, 12616 (2019).